Available online at www.sciencedirect.com
ScienceDirect
Journal of Hazardous Materials 150 (2008) 62–67
Journal of Hazardous Materials
www.elsevier.com/locate/jhazmat

Photoinduced hydroxyl radical and photocatalytic activity of samarium-doped TiO_2 nanocrystalline

Qi Xiao *, Zhichun Si, Jiang Zhang, Chong Xiao, Xiaoke Tan

School of Resources Processing and Bioengineering, Central South University, Changsha 410083, China

Received 1 February 2007; received in revised form 21 March 2007; accepted 17 April 2007
Available online 20 April 2007

Abstract

Sm^{3+}-doped TiO_2 nanocrystalline has been prepared by sol–gel auto-combustion technique and characterized by X-ray diffraction (XRD), Brunauer–Emmett–Teller (BET) method, and also UV–vis diffuse reflectance spectroscopy (DRS). These Sm^{3+}-doped TiO_2 samples were tested for methylene blue (MB) decomposition and $^{\bullet}OH$ radical formation. The analysis of $^{\bullet}OH$ radical formation on the sample surface under UV irradiation was performed by fluorescence technique with using terephthalic acid, which readily reacted with $^{\bullet}OH$ radical to produce highly fluorescent product, 2-hydroxyterephthalic acid. It was observed that the presence of Sm^{3+} ion as a dopant significantly enhanced the photocatalytic activity for MB degradation under UV light irradiation because both the larger specific surface area and the greater the formation rate of $^{\bullet}OH$ radical were simultaneously obtained for Sm^{3+}-doped TiO_2 nanocrystalline. The adsorption experimental demonstrated that Sm^{3+}-TiO_2 had a higher MB adsorption capacity than undoped TiO_2 and the adsorption capacity of MB increased with the increase of samarium ion content. The results also indicated that the greater the formation rate of $^{\bullet}OH$ radical was, the higher photocatalytic activity was achieved. In this study, the optimum amount of Sm^{3+} doping was 0.5 mol%, at which the recombination of photo-induced electrons and holes could be effectively inhibited, the highest formation rate of $^{\bullet}OH$ radicals was, and thereby the highest photocatalytic activity was achieved.

Keywords: Sm^{3+}-doped TiO_2 nanocrystalline; Hydroxyl radical; Photocatalytic activity

1. Introduction

TiO_2 photocatalyst has attracted a great deal of attention in environmental wastewater treatment in the past decade, because it generates highly oxidative hydroxyl free radicals ($^{\bullet}OH$), which can degrade many toxic and non-biodegradable organics [1–3]. Previous studies indicated that the photocatalytic activity of TiO_2 catalysts depended strongly on two factors: adsorption behavior and the separation efficiency of electron–hole pairs [1,2]. The adsorption capacity can be generally improved by increasing the specific surface area of catalysts. On the other hand, in order to eliminate the recombination rate of the electron–hole pairs, several approaches have been proposed, including transition metals doping [3,4], coupling with other semiconductors [5,6], noble metals deposition [7] and rare earth ions doping [8–11]. Especially, the photocatalytic activity of TiO_2 could be significantly enhanced by doping with lanthanide ions with 4f configurations because lanthanide ions could form complexes with various Lewis bases including organic acids, amines, aldehydes, alcohols, and thiols in the interaction of the functional groups with their f-orbital [12–14]. Xu et al. [12] reported that doping with La^{3+}, Ce^{3+}, Er^{3+}, Pr^{3+}, Gd^{3+}, Nd^{3+}, or Sm^{3+} was beneficial to NO_2 adsorption. Ranjit et al. [13,14] reported that doping with Eu^{3+}, Pr^{3+}, or Yb^{3+} increased the adsorption capacity and also adsorption rate of TiO_2 catalysts simultaneously in aqueous salicylic acid, *t*-cinnamic acid, and *p*chlorophenoxy–acetic acid solutions. Thus, doping with lanthanide ions could provide a means to concentrate on the organic pollutant at the semiconductor TiO_2 surface and therefore enhance the photoactivity of titania [15,16]. On the other hand, doping with lanthanide ions with 4f electron configurations also could significantly improve the separation rate of photo-induced charge carriers in TiO_2 photocatalysts and greatly enhance the photocatalytic activity of TiO_2 [8–11]. Wang and his co-workers reported that the separation of electron–hole pairs was more efficient in the lanthanide ion-doped TiO_2 including

* Corresponding author. Tel.: +86 731 8830543; fax: +86 731 8879815.
E-mail address: xiaoqi88@mail.csu.edu.cn (Q. Xiao).

0304-3894/$ – see front matter © 2007 Elsevier B.V. All rights reserved.
doi:10.1016/j.jhazmat.2007.04.045

La^{3+}, Nd^{3+}, Pr^{3+}, Sm^{3+}, and Eu^{3+} than that in pure TiO_2 [17,18]. Li et al. [19] reported that the introduction of Ce 4f level led to eliminate the recombination of electron–hole pairs and enhance the photocatalytic activity.

•OH radicals have been proposed to be the responsible for many oxidation pathways of chemical compounds initiated through heterogeneous photocatalytic processes [1]. Accordingly, •OH radicals as much as possible are required to be generated on the TiO_2 surface in order to increase the reactivity. The yield of •OH radicals depends on the competition between oxidation of surface water by the holes and electron–hole recombination. Therefore, the measurement of the formation rate of the hydroxyl radical is considered to give more important information to help understand the role of lanthanide ions doping in increase of photocatalytic activity. However, there are few papers about the effect of lanthanide ions doped TiO_2 on the amount of the •OH radicals formation.

In the present work, the model dye was methylene blue (MB), which was often used as a standard target compound in a test of photocatalysts. Moreover, a detailed photocatalytic degradation pathway of MB has been determined by a careful identification of intermediate products, and the photocatalytic reaction was found to proceed preferably through the oxidation of MB by the generated •OH radicals [20]. Fluorescence technique was applied to the detection of •OH radicals formed on a photo-illuminated TiO_2 surface using terephthalic acid which readily reacted with to produce highly fluorescent products. Previous studies [21] have demonstrated the possibility of using this method to quantify the complete hydroxyl radical production from the photogenerated holes at the semiconductor surface. In addition, the Sm^{3+}-doped TiO_2 samples were characterized by X-ray diffraction (XRD), UV–vis diffuse reflectance spectroscopy. The aim of this study was to examine and correlate the photocatalytic degradation of MB with •OH radicals formed on Sm^{3+}-doped TiO_2 samples, and disclose the mechanisms of photocatalytic activity enhancement due to samarium ion doping by investigating the effects of samarium ion doping on the separation of electron–hole pairs under either UV light irradiation.

2. Experimental

2.1. Synthesis of Sm^{3+}-doped TiO_2 nanocrystalline

Sm^{3+}-doped TiO_2 nanocrystalline was synthesized by a sol–gel auto-combustion method. The detailed process can be described as follows. The analytical grade titanium isopropoxide (Ti $(OPr^i)_4$), Sm $(NO_3)_3$, $C_2H_6O_2$ (ethylene glycol, abbreviated as EG), $C_6H_8O_7$ (citric acid, abbreviated as CA), ammonia (25%) and nitride acid (65%–68%) were used as raw materials. Appropriate amount of Ti $(OPr^i)_4$ and Sm $(NO_3)_3$ were added to CA and EG mixture under constant stirring condition. The amounts of doped Sm^{3+} were 0.5–1.5 mol%. The molar ratios of CA/Ti and CA/EG were kept constant at 2:1 and 1:1, respectively. After adjusting the pH value with ammonia to 6–7, the mixture solution was evaporated at 90 °C to gradually form a clear precursor gel. The precursor gel was baked at 150 °C in muffle furnace and expanded, then was auto-ignited at about 250 °C. The puffy, porous gray powders were calcined at 600 °C for 2 h in air.

2.2. Characterization of Sm^{3+}-doped TiO_2 nanocrystalline

The crystalline structure of the samples was determined by a *D*/max-γA diffractometer (Cu Kα radiation, $\lambda = 0.154056$ nm) studies. The averaged grain sizes D were determined from the XRD pattern according to the Scherrer equation $D = K\lambda/\beta\cos\theta$, where k is a constant (shape factor, about 0.9), λ is the X-ray wavelength (0.15418 nm), β the full width at half maximum (FWHM) of the diffraction line, and θ the diffraction angle. The values of β and θ of anatase and rutile were taken from anatase (1 0 1) and rutile (1 1 0) diffraction line, respectively. The amount of rutile in the samples was calculated using the following equation [22]: $X_R = (1 + 0.8I_A/I_R)^{-1}$, where X_R is the mass fraction of rutile in the samples, I_A and I_R were the X-ray integrated intensities of (1 0 1) reflection of the anatase and (1 1 0) reflection of rutile, respectively.

The specific surface area of the powders was measured by the dynamic Brunauer–Emmett–Teller (BET) method, in which a N_2 gas was adsorbed at 77 K using a Micromeritics ASAP 2000 system. The diffuse reflectance spectra (DRS) of the photocatalyst sample in the wavelength range of 200–800 nm were obtained using a UV–vis scanning spectrophotometer (Shimadzu UV-3101) and were converted from reflectance to absorbance by the Kubelka–Munk method.

2.3. Determination of •OH radicals

The analysis of •OH radical's formation on the sample surface under UV irradiation was performed by fluorescence technique with using terephthalic acid, which readily reacted with •OH radicals to produce highly fluorescent product, 2-hydroxyterephthalic acid [21]. The intensity of the peak attributed to 2-hydroxyterephtalic acid was known to be proportional to the amount of •OH radicals formed [21]. The selected concentration of terephthalic acid solution was 5×10^{-4} M in a diluted NaOH aqueous solution with a concentration of 2×10^{-3} M. It has been proved that under these experimental conditions (low concentration of terephthalic acid, less than 10^{-3} M, room temperature), the hydroxylation reaction of terephthalic acid proceeds mainly by •OH radicals [21].

Two hundreds milligrams of the prepared Sm^{3+}-doped TiO_2 samples was added to 200 mL of the 5×10^{-4} M terephthalic acid solution in 2×10^{-3} M NaOH, and then UV irradiation of the solution was started. For UV irradiation, a 160 W high-pressure mercury lamp (GYZ-160) fixed at a distance of 150 mm above the surface solution was used as UV light source. Sampling was performed in every 15 min. Solution after filtration through 0.45 μm membrane filter was analyzed on a Hitachi F-4500 fluorescence spectrophotometer. The product of terephthalic acid hydroxylation, 2-hydroxyterephthalic acid, gave a peak at the wavelength of about 425 nm by the excitation with the wavelength of 315 nm.

2.4. MB adsorption experiment

To determine the adsorption behavior of Sm^{3+} ion doped and pure TiO_2 catalyst, a set of adsorption isotherm tests in the dark was performed. In each test, 0.02 g of catalyst was added to 20 mL of MB aqueous solution. The mixture was well dispersed, and put in the dark for 24 h at 298 ± 1 K. The MB concentration in the suspension before and after the adsorption tests was analyzed and the adsorbed amount of MB on the catalysts was calculated based on a mass balance.

2.5. Photocatalytic degradation of MB

In order to evaluate photocatalytic activity of the prepared samples, photocatalytic degradation of MB was performed. For a typical photocatalytic experiment, 200 mg of the prepared Sm^{3+}-doped TiO_2 nanocrystalline was added to 200 mL of the 100 ppm MB aqueous solution. The prepared Sm^{3+}-doped TiO_2 nanocrystalline was dispersed under ultrasonic vibration for 10 min. After keeping at least 20 min, MB concentration in the solution was found to be constant on all samples prepared. Therefore, the solution in which the prepared Sm^{3+}-doped TiO_2 nanocrystalline was dispersed was kept in the dark for 30 min and then UV irradiation of the solution was started. For UV irradiation, a 160 W high-pressure mercury lamp (GYZ-160) fixed at a distance of 150 mm above the surface solution was used as UV light source. The light absorption of solution after filtration through 0.45 μm membrane filter was measured at 664 nm (λ_{max} for MB) at a set time. The decolorization of MB was calculated by formula: Decolorization = $(C_0 - C)/C_0$, where C_0 and C is the concentration of the primal and remaining MB, respectively, and $(C_0 - C)$ is the concentration of the decomposed MB. The absorbance of the MB solution was measured with a UV–vis spectrophotometer (Shimadzu UV-3101).

3. Results and discussion

3.1. XRD analysis

XRD patterns of Sm^{3+}-doped TiO_2 nanocrystalline with various samarium content calcined at 600 °C for 2 h were shown in Fig. 1. From these XRD results, it was shown that the X-ray diffraction peak at 25.5° corresponded to characteristic peak of crystal plane (1 0 1) of anatase, and the peak at 27.6° corresponded to characteristic peak of crystal plane (1 1 0) of rutile. In undoped titania sample calcined at 600 °C for 2 h, rutile was the dominant crystallized phase, and the sample contains 97.5% of rutile phase, while Sm^{3+}-doped TiO_2 samples showed a mixture phase of anatase and rutile, and the relative ratio of rutile to anatase was reduced with the increase of samarium content, showing that the anatase-to-rutile phase transformation was greatly inhibited by samarium ion doping. Lin et al. [23,24] also found that other rare earth ions (La, Y, and Ce) could inhibited the anatase-to-rutile phase transformation during the thermal treatment. The inhibition of the phase transition was ascribed to the stabilization of the anatase phase by the surrounding rare earth ions through the formation of Ti–O–rare-earth element bonds [25]. In the present system, I thought that the likely formation of Sm–O–Ti interaction took place and inhibited the transition of the anatase phase. But the mechanism dominating in the anatase-to-rutile phase transformation process was complex and not fully understood yet. Therefore, the more detailed study should be done in the future in order to extensively understand the effect of samarium ion doping on the anatase-to-rutile phase transformation.

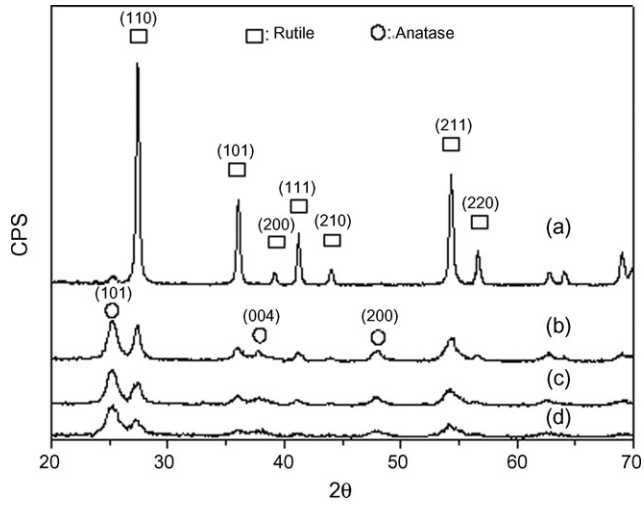

Fig. 1. XRD patterns of TiO_2 with various amounts of samarium calcined at 600 °C for 2 h.

3.2. Diffuse reflectance spectra

To investigate the optical absorption properties of catalysts, the diffuse reflectance spectra (DRS) of TiO_2 and Sm^{3+}-doped TiO_2 in the range of 220–850 nm was examined and the results were shown in Fig. 2. It was shown that while TiO_2 had no absorption in the visible region (>400 nm), Sm^{3+}-doped TiO_2 had significant absorption between 400 and 500 nm, which increased with the increase of samarium ion content. In addition, the optical absorption in the UV region was also enhanced. Li et al. [26] reported that the band gap of TiO_2 nanoparticles

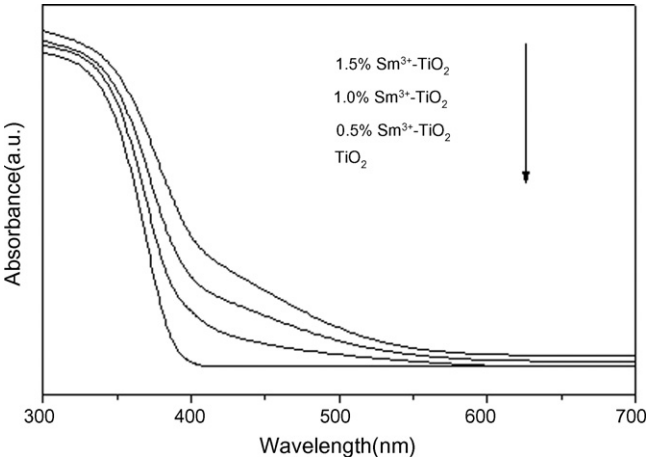

Fig. 2. UV–vis absorption spectra of pure and doped TiO_2 calcined at 600 °C for 2 h.

Table 1
The characteristics of Sm^{3+}-doped samples containing different samarium content calcined at 600 °C

Samarium content %	Anatase		Rutile		Specific surface area (m^2/g)	Decolourization of MB at 120 min (%)
	Crystal size $D_{(101)}$ (nm)	X_A (%)	Crystal size $D_{(110)}$ (nm)	X_R (%)		
0	–	2.41	18.8	97.59	24.52	65.3
0.5	13.8	48.39	13.6	51.61	52.75	95.6
1.0	12.9	58.22	13.1	41.78	69.48	88.8
1.5	12.5	58.33	12.8	41.67	82.94	73.9

was reduced by Nd^{3+} doping and the band gap narrowing was primarily attributed to the substitution Nd^{3+} ions which introduced electron states into the band gap of TiO_2 to form the new lowest unoccupied molecular orbital. In order to understand the reason of the band gap narrowing for Sm^{3+}-doped TiO_2, density functional theory calculations were in going.

3.3. Adsorption behavior of methylene blue

The BET results (shown in Table 1) showed that the specific surface areas of the catalysts significantly increased from 24.52 $m^2\,g^{-1}$ for TiO_2 to 82.94 $m^2\,g^{-1}$ for 1.5% Sm^{3+}–TiO_2. The larger specific surface area of Sm^{3+}-doped TiO_2 nanocrystalline would be beneficial to achieve better adsorption of MB in aqueous suspension. The MB adsorption isotherms were shown in Fig. 3. It was shown that the Sm^{3+}-doped TiO_2 nanocrystalline had a higher MB adsorption capacity than undoped TiO_2. While the saturated adsorption amount of MB onto the TiO_2 was 0.8262×10^{-7} mol m^{-2}, the saturated adsorption amount of MB onto the Sm^{3+}-doped TiO_2 nanocrystalline increased with the increase of samarium ion content up to 1.0887×10^{-7} mol m^{-2}.

3.4. Formation of •OH radicals

The fluorescence emission spectrum (excitation at 315 nm) of terephthalic acid solution was measured every 15 min during illumination. Fig. 4 showed the induction of fluorescence from 5×10^{-4} M terephthalic acid solution in 2×10^{-3} M NaOH. As shown in the figures, gradual increase in the fluorescence intensity at about 425 nm was observed with increasing illumination time. Based on the reports in radiation chemistry [27] and sonochemistry [28–30], it was reasonable to assume that photogenerated O_2^-, $HO_2^•$ and H_2O_2 did not interfere with the reaction between •OH and terephthalic acid. Moreover, the generated spectrum had the identical shape and maximum wavelength with that of 2-hydroxyterephthalic acid. These results suggested that fluorescent products formed during 0.5% Sm^{3+}–TiO_2 photocatalysis were due to the specific reaction between •OH radicals and terephthalic acid.

Fig. 5 showed the plots of increase in fluorescence intensity against illumination time at 425 nm. The fluorescence intensity by UV light illumination in terephthalic acid solutions increased almost linearly against time. Consequently, we can conclude that •OH radicals formed at the TiO_2 interface are in proportional to the light illumination time obeying zero-order reaction rate kinetics. The formation rate of the •OH radicals could be expressed by the slop of these lines shown in Fig. 5. According to Fig. 5, the order of the formation rate of •OH radicals formed on the Sm^{3+}-doped TiO_2 nanocrystalline was as following: 0.5 > 1.0 > 1.5 > 0 mol%, which suggested that the Sm^{3+} doping enhanced the formation rate of •OH radicals and there was an optimum doping content of Sm^{3+} ions in TiO_2 particles.

Absorption of a photon with energy greater than the band gap energy resulted in the formation of conduction band electron and valence band hole, according to reaction (1). It was commonly

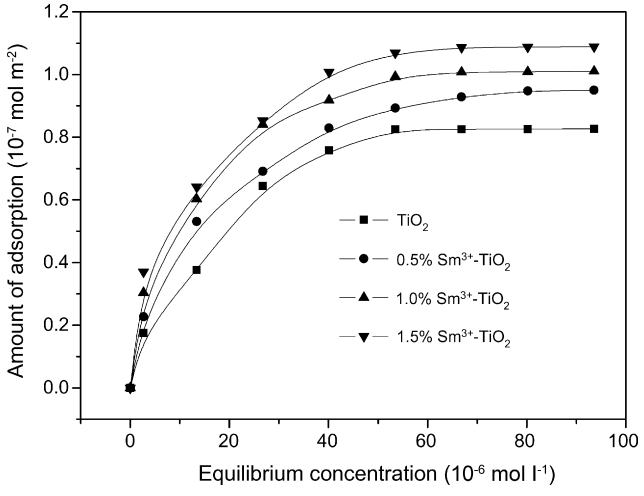

Fig. 3. The MB adsorption isotherms on the pure and doped TiO_2.

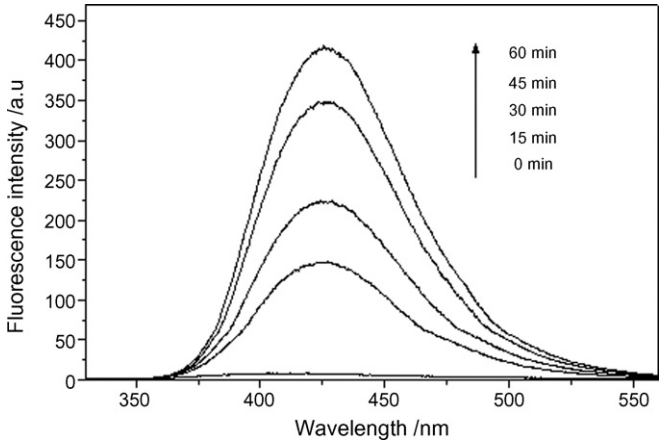

Fig. 4. Fluorescence spectral changes observed during illumination of 0.5% Sm^{3+}–doped TiO_2 in 4×10^{-4} M NaOH solution of terephthalic acid (excitation at 315 nm). Each fluorescence spectrum was recorded every 15 min of UV illumination.

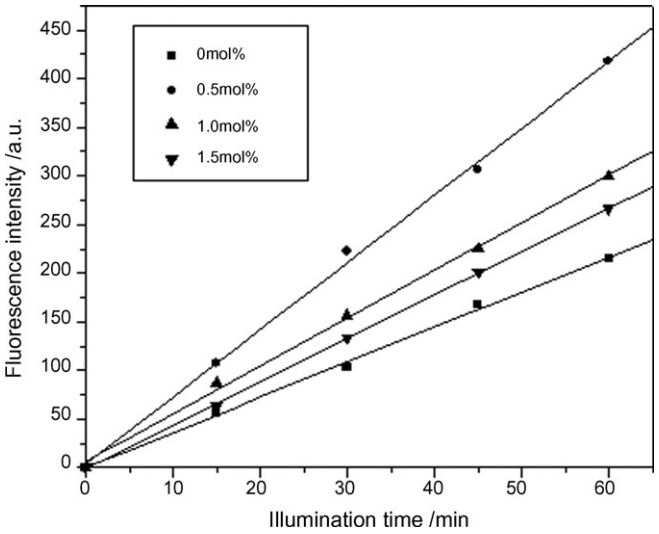

Fig. 5. Plots of the induced fluorescence intensity at 426 nm against irradiation time for terephthalic acid on samarium doped TiO_2.

accepted that the hole was quickly converted to the hydroxyl radical upon oxidation of surface water, according to reaction (2), and that the hydroxyl radical was the major reactant, which was responsible for oxidation of organic substrates. The yield of $^{\bullet}OH$ radicals depended on the competition between oxidation of surface water by the holes (reaction (2)) and electron–hole recombination according to reaction (3). Therefore, the greater the formation rate of $^{\bullet}OH$ radicals was the higher separation efficiency of electron–hole pairs was achieved. All above-mentioned results demonstrated that Sm^{3+} doping could effectively enhance the separation efficiency of electron–hole pairs, and in this study the optimum doping content of Sm^{3+} in the titania was found be 0.5 mol%, at which the recombination of photo-induced electrons and holes could be the most effectively inhibited, which was in accordance with the previous results [12]. Xu et al. [12] reported that there existed an optimum doping content of rare earth ions in TiO_2 particles for the most efficient separation of photo-induced electron–hole pairs.

$$TiO_2 \xrightarrow{h\nu} e_{TiO_2^-} + h^+ \quad (1)$$

$$h^+ + H_2O_{ads} \rightarrow {}^{\bullet}OH_{ads} \quad (2)$$

$$h^+ + e_{TiO_2^-} \rightarrow TiO_2 \quad (3)$$

3.5. Photocatalytic activity

The photocatalytic degradation of MB over Sm^{3+}-doped TiO_2 samples calcined at 600 °C with different content of Sm^{3+} ion was evaluated and the results were shown in Fig. 6. According to Fig. 6, the order of photocatalytic activity of Sm^{3+}-doped TiO_2 nanocrystalline at 120 min was as followings: 0.5 > 1.0 > 1.5 > 0 mol%, which suggested that the Sm^{3+} doping enhanced the photocatalytic activity of TiO_2 and there was an optimum doping content of Sm^{3+} ions in TiO_2 particles.

The photocatalytic activity of TiO_2 catalysts depended strongly on two factors: adsorption behavior and the separation efficiency of electron–hole pairs [1,31,32].

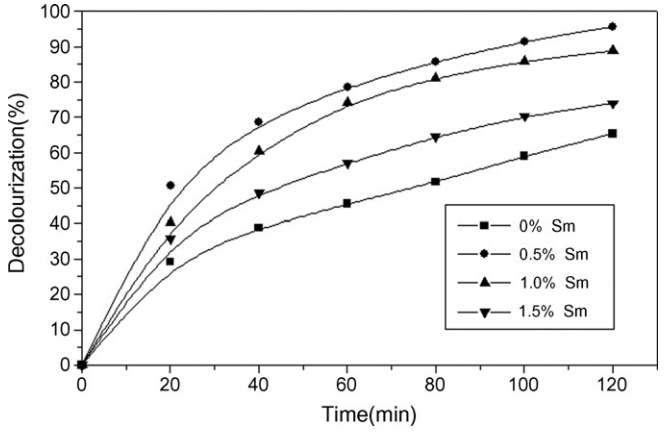

Fig. 6. Photocatalytic decomposition profiles of methylene blue over different samarium doped TiO_2 nanoparticle calcined at 600 °C for 2 h.

The photo-induced electron transferred to adsorbed organic species resulted from migration of electrons and holes to the semiconductor surface. The electron transfer process was more efficient if the species were pre-adsorbed on the surface [32]. According to Figs. 3 and 6, the photocatalytic reactivity of Sm^{3+}–TiO_2 was higher than that of undoped TiO_2, which was consistent with the higher adsorption capacity of Sm^{3+}–TiO_2 than undoped TiO_2. However, it was noticeable that a higher adsorption capacity with a higher samarium ion dosage did not lead to a higher photocatalytic activity, which might be limited by lower separation efficiency of electron–hole pairs.

On the other hand, according to Figs. 5 and 6, it was found that the order of photocatalytic activity was the same as that of the formation rate of $^{\bullet}OH$ radicals, namely, the greater the formation rate of $^{\bullet}OH$ radicals was, the higher photocatalytic activity was achieved, indicating that the photocatalytic activity was positive correlation to the formation rate of $^{\bullet}OH$ radicals on the catalysts. During the photocatalytic process, the absorption of photons by the photocatalysts led to the excitation of electrons from the valence band to the conduction band, thus generating electron–hole pairs. Oxygen molecules dissolved in the suspension captured the electron in the conduction band, and the hole in the valence band was captured by H_2O species adsorbed on the surface of the catalysts, to produce the $^{\bullet}OH$ radicals, which subsequently oxidized an adsorbed pollutants. According to Houas et al. [20], firstly the $^{\bullet}OH$ radical generated through the oxidation of water molecules adsorbed on TiO_2, and then $^{\bullet}OH$ radical oxidized the adsorbed MB molecules. For that reason, the greater the formation rate of $^{\bullet}OH$ radicals was, the higher photocatalytic activity was achieved. Therefore, in this study 0.5 mol% was the optimum content of Sm^{3+} in the titania, at which the recombination of photo-induced electrons and holes could be effectively inhibited, the highest formation rate of $^{\bullet}OH$ radicals arrived at, and thereby the highest photocatalytic activity was achieved.

4. Conclusions

It was observed that the presence of Sm^{3+} ion as a dopant significantly improved the photocatalytic activity for MB degra-

dation under UV light irradiation because both the larger specific surface area and the greater the formation rate of •OH radical were simultaneously obtained for Sm^{3+}-doped TiO_2 nanocrystalline. Sm^{3+}–TiO_2 had a higher MB adsorption capacity than undoped TiO_2. The photocatalytic activity was positive correlation to the formation rate of •OH radicals, namely, the greater the formation rate of •OH radicals was, the higher photocatalytic activity was achieved. In this study, the optimum amount of Sm^{3+} doping was 0.5 mol%, at which the recombination of photo-induced electrons and holes could be effectively inhibited, the highest formation rate of •OH radicals was, and thereby the highest photocatalytic activity was achieved.

Acknowledgements

This work was supported by the Provincial Excellent PhD Thesis Research Program of Hunan (No.2004-141) and the Postgraduate Educational Innovation Engineering of Central South University (No.2005-22).

References

[1] M.R. Hoffmann, S.T. Choi, W. Martin, D.W. Bahnemann, Environmental applications of semiconductor photocatalysis, Chem. Rev. 95 (1995) 69.
[2] A. Fujishima, T.N. Rao, D.A. Truk, Titanium dioxide photocatalysis, J. Photochem. Photobiol. C: Photochem. Rev. 1 (2000) 1.
[3] W. Choi, A. Termin, M.R. Hoffmann, The role of metal ion dopants in quantum-sized TiO_2: correlation between photoreactivity and charge carrier recombination dynamics, J. Phys. Chem. 98 (1994) 13669.
[4] D.H. Kim, S.I. Woo, S.H. Moon, H.D. Kim, B.Y. Kim, J.H. Cho, Y.G. Joh, E.C. Kim, Effect of Co/Fe co-doping in TiO_2 rutile prepared by solid state reaction, Solid State Commun. 136 (2005) 554.
[5] A. Hattori, Y. Tokihisa, H. Tada, S. Ito, Acceleration of oxidations and retardation of reductions in photocatalysis of a TiO_2/SnO_2 pilayer-type catalyst, J. Electrochem. Soc. 147 (2000) 2279.
[6] C. Wang, B.-Q. Xu, X. Wang, J. Zhao, Preparation and photocatalytic activity of $ZnO/TiO_2/SnO_2$ mixture, J. Solid State Chem. 178 (2005) 3500.
[7] F.B. Li, X.Z. Li, Photocatalytic properties of gold/gold ion-modified titanium dioxide for wastewater treatment, Appl. Catal. A: Gen. 228 (2002) 15.
[8] L. Jing, X. Sun, B. Xin, B. Wang, W. Cai, H. Fu, The preparation and characterization of La doped TiO_2 nanoparticles and their photocatalytic activity, J. Solid State Chem. 177 (2004) 3375.
[9] Y. Zhang, H. Xu, Y. Xu, H. Zhang, Y. Wang, The effect of lanthanide on the degradation of RB in nanocrystalline Ln/TiO_2 aqueous solution, J. Photochem. Photobiol. Chem. 170 (2005) 279.
[10] X. Yan, J. He, D.G. Evans, X. Duan, Y. Zhu, Preparation, characterization and photocatalytic activity of Si-doped and rare earth-doped TiO_2 from mesoporous precursors, Appl. Catal. B: Environ. 55 (2005) 243.
[11] Y. Xie, C. Yuan, X. Li, Photosensitized and photocatalyzed degradation of azo dye using Ln^{n+}–TiO_2 sol in aqueous solution under visible light irradiation, Mater. Sci. Eng., B 117 (2005) 325.
[12] A.-W. Xu, Y. Gao, H.-Q. Liu, The preparation, characterization, and their photocatalytic activities of rare-earth-doped TiO_2 nanoparticles, J. Catal. 207 (2002) 151.
[13] K.T. Ranjit, I. Willner, S.H. Bossmann, A.M. Braun, Lanthanide oxide doped titanium dioxide photocatalysts: effective photocatalysts for the enhanced degradation of salicylic acid and *t*-Cinnamic acid, J. Catal. 204 (2001) 305.
[14] K.T. Ranjit, I. Willner, S.H. Bossmann, A.M. Braun, Lanthanide oxide-doped titanium dioxide photocatalysts: novel photocatalysts for the enhanced degradation of *p*-Chlorophenoxyacetic acid, Environ. Sci. Technol. 35 (2001) 1544.
[15] D.W. Hwang, J.S. Lee, W. Li, S.H. Oh, Electronic band structure and photocatalytic activity of $Ln_2Ti_2O_7$ (Ln = La, Pr, Nd), J. Phys. Chem. B 107 (2003) 4963.
[16] Y.H. Zhang, H.X. Zhang, Y.X. Xu, Y.G. Wang, Europium doped nanocrystalline titanium dioxide: preparation, phase transformation and photocatalytic properties, J. Mater. Chem. 13 (2003) 2261.
[17] Y.Q. Wang, H.M. Cheng, Y.Z. Hao, J.M. Ma, W.H. Li, S.M. Cai, Photo-electrochemical properties of metal-ion-doped TiO_2 nanocrystalline electrodes, Thin Solid Films 349 (1999) 120.
[18] Y.Q. Wang, H.M. Cheng, Y.Z. Hao, J.M. Ma, W.H. Li, S.M. Cai, Photoelectrochemistry of Nd^{3+}-doped TiO_2 nanocrystalline electrodes, J. Mater. Sci. Lett. 18 (1999) 127.
[19] F.B. Li, X.Z. Li, M.F. Hou, K.W. Cheah, W.C.H. Choy, Enhanced photocatalytic activity of Ce^{3+}–TiO_2 for 2-mercaptobenzothiazole degradation in aqueous suspension for odour control, Appl. Catal. Gen. 285 (2005) 181.
[20] A. Houas, H. Lachheb, M. Ksibi, E. Elaloui, C. Guillard, J.-M. Herrmann, Photocatalytic degradation pathway of methylene blue in water, Appl. Catal. B Environ. 31 (2001) 145.
[21] K. Ishibashi, A. Fujishima, T. Watanabe, K. Hashimoto, Detection of active oxidative species in TiO_2 photocatalysis using the fluorescence technique, Electrochem. Commun. 2 (2000) 207.
[22] R.A. Spurr, H. Myers, Quantitative analysis of anatase-rutile mixtures with an X-Ray diffractometer, Anal. Chem. Technol. 29 (1957) 760.
[23] J. Lin, J.C. Yu, D. Lo, S.K. Lam, Photocatalytic activity of rutile $Ti_{1-x}Sn_xO_2$ solid solutions, J. Catal. 183 (1999) 368.
[24] J. Lin, J.C. Yu, An investigation on photocatalytic activities of mixed TiO_2-rare earth oxides for the oxidation of acetone in air, J. Photochem. Photobiol. Chem. 116 (1998) 63.
[25] E.L. Crepaldi, G.J. de, A.A. Soler-Illia, D. Grosso, F. Cagnol, F. Ribot, C. Sanchez, Controlled formation of highly organized mesoporous titania thin films: from mesostructured hybrids to mesoporous nanoanatase TiO_2, J. Am. Chem. Soc. 125 (2003) 9770.
[26] W. Li, Y. Wang, H. Lin, S. Ismat Shah, C.P. Huang, D.J. Doren, A. Sergey, J.G. Rykov, M.A. Chen, Barteau, Band gap tailoring of Nd^{3+}-doped TiO_2 nanoparticles, Appl. Phys. Lett. 83 (2003) 4143.
[27] H.M. Khan, M. Anwar, G. Ahmad, Effect of temperature and light on the response of an aqueous coumarin dosimeter, J. Radioanal. Nucl. Chem. Lett. 200 (1995) 521.
[28] T.J. Mason, J.P. Lorimer, D.M. Bates, Y. Zhao, Dosimetry in sonochemistry: the use of aqueous terephthalate ion as a fluorescence monitor, Ultrason. Sonochem. 1 (1994) S91.
[29] X. Fang, G. Mark, Clemens von Sonntag, OH radical formation by ultrasound in aqueous solutions part 1: the chemistry underlying the terephthalate dosimeter, Ultrason. Sonochem. 3 (1996) 57.
[30] J.C. Barreto, G.S. Smith, N.H.P. Strobel, P.A. McQuillin, T.A. Miller, Terephthalic acid: A dosimeter for the detection of hydroxyl radicals in vitro, Life Sci. 56 (1994) L89.
[31] H. Liu, S. Cheng, M. Wu, H. Wu, J. Zhang, W. Li, C. Cao, Photoelectrocatalytic degradation of sulfosalicylic acid and its electro-chemical impedance spectroscopy investigation, J. Phys. Chem. A 104 (2000) 7016.
[32] A.L. Linsebigler, G. Lu, J.T. Yates, Photocatalysis on TiO_2 surfaces principles, mechanisms, and selected results, Chem. Rev. 95 (1995) 735.